Journal of Applied Fluid Mechanics, Vol. 12, No. 4, pp. 1083-1091, 2019.
Available online at www.jafmonline.net, ISSN 1735-3645, EISSN 1735-3645.
DOI: 10.29252/jafm.12.04.29694

Finite Element Analysis of Pulsatile Blood Flow in Elastic Artery

O. Elbanhawy[1,2], A. Guaily[2,3†] and M. Tosson[2]

[1] *University of Guelph, Guelph, Ontario, N1G 2W1, Canada*
[2] *Cairo University, Giza, Giza, 12613, Egypt*
[3] *Nile University, Shaikh Zaid, Giza, 12588, Egypt*

†*Corresponding Author Email: aguaily@nu.edu.eg*

(Received October 5, 2018; accepted December 4, 2018)

ABSTRACT

New hybrid Eulerian/Lagrangian model is presented accounting for the two-way coupling between the pulsating blood flow and the artery deformability. The Streamline-Upwind/Petrove--Galerkin (SUPG) finite element technique is used to treat for the convective nature of the momentum equation. The deformability of the artery walls is accounted for by treating the wall as an elastic beam under transverse unsteady distributed load, namely the fluid pressure. The results of the present contribution compare well against the available published data.

Keywords: Fluid structure interaction; Incompressible viscous flows; Pulsating flows; Deformable boundaries.

NOMENCLATURE

ALE	arbitrary Lagrangian-Eulerian
D	inlet diameter
E	modulus of elasticity
G	gradient operator
I	moment of area
IFSI	index of Fluid-Structure Interaction
k	artificial diffusivity coefficient
$\mathbf{V}$	velocity vector
M	mass matrix
N	weighting function
P	pressure
p	discontinuous streamline upwind contribution
q	vertical load
R_e	Reynold's number
t	time
U	potential Energy
w	vertical deflection
x	longitudinal direction
α	Womersley number
ρ	blood density
μ	blood viscosity
ε	pressure stabilization controlling Parameter
θ	slope of the deflection
ω	frequency

1. INTRODUCTION AND LITERATURE SURVEY

Modeling and simulation of fluid-structure interaction is one of the most challenging problems. Survey of literature reveals that treating the boundary deformability could be divided into three approaches depending on the utilized computational framework. The simplest one is linearized kinematics approach, in which the Eulerian frame is used for both fluid and wall equations (Deparis *et al.*, 2003; Fernández and Tallec, 2003; Figueroa *et al.*, 2006; Mao *et al.*, 2017; Sugiyama *et al.*, 2017). In this framework, the interface between the fluid and the tube walls is fixed but the nodes have non-zero velocities. Deparis *et al.* (2003) proposed a modified fixed-point algorithm with a transpiration formulation to reduce the computational time. Fernández and Tallec (2003) also used the linearization principle with a reduced linear structure to solve problems of fluid-structure interaction. Figueroa *et al.* (2006) developed the coupled momentum method by adopting the linearized kinematics formulation for the tube walls. This method couples the elastodynamic equations of the tube walls to the Navier--Stokes equations using a shear-enhanced membrane model for the

vessel walls. The second computational framework is the immersed boundary method (Peskin, 1977; Hart *et al.*, 2003; Enriquez-Remigio and Roma, 2005). This computational approach is implemented in the areas where the mass of the solid is insignificant compared to the mass of the fluid and can be ignored. This approach is used in modeling of the flow across heart valves and inside the heart itself. The third computational framework is the Arbitrary Lagrangian-Eulerian (ALE) formulation for fluid-solid interaction problems (Hughes and Zimmermann, 1981; Donea *et al.*, 1982; Kelidis and Konstantinidis, 2018). In this framework, the flow domain is no longer fixed. The wall deformation problem is solved in Lagrangian formulation, and the grid is updated each time step. ALE formulation is computationally expensive when considering large models of the vasculature and less robust than linearized kinematics methods since they necessitate the continual updating of the grid. Recently, new direction for bubbly flows has been introduced using direct numerical simulations (Ma *et al.*, 2015; Ma *et al.*, 2016; Tryggvason *et al.*, 2016) in which closure terms for a simple model of the average flow are found, using Neural Networks. Popine and Zaleski (1999) focused on obtaining an accurate description of the surface tension terms by considering a front tracking algorithm for incompressible flows while Bo *et al.* (2011) presented a robust front tracking method for compressible flows in which they combined the best features of a front tracking method and a ghost fluid method. In the present work, the deformability of the boundary is accounted for by considering the boundary as a simply supported beam under transverse unsteady distributed load, namely the fluid pressure. The principal of minimum potential energy in elasticity in the case of bending in the regime of small deflections is used to model the boundary deflection. The proposed approach is explained in detail in section 2 and is tested by simulating a typical pulsatile blood flow in a deformable artery. Which shall provide better understanding and guidance for the medical decisions that depend on the values of the pressure as well as the wall shear stresses. Another potential application is the study of the effect of the substratum deformability on the growth rate of the biofilm (Kelly *et al.*, 2013; Boraey *et al.*, 2015). Industrial flow regulator (Raju *et al.*, 2017) could be considered as another important application. Solving the Navier--Stokes equations is a real challenge due to the convective nature of the equations which necessitates the use of stabilization techniques. Several techniques have been proposed to stabilize the classical finite element method for convection–diffusion problems. As one of the earliest efforts in this field, one can mention the least-squares (LS) technique presented by Lynn and Arya (1973). The main advantage of the LS technique is that it produces a symmetric and positive definite coefficient matrix when applied to first order partial differential equations (Guaily and Epstein, 2010). The main drawback of the LS technique is that it produces excessive artificial diffusion in all directions as explained by Taghaddosi *et al.* (1999). To obtain satisfactory results with the LS method one can adapt the grid to the flow regions with high gradients (Ait-Ali-Yahia *et al.*, 1996; Guaily and Megahed, 2010). As a remedy for this flaw, the streamline-upwind Petrov/Galerkin (SUPG) method was developed by Brooks and Hughes (1982) which produces diffusion in a specific direction namely, the streamline direction. Then Hughes and Franca (1989) presented the Galerkin/least-squares (GLS) technique which represents a conceptual simplification of SUPG. It is worth mentioning that both the SUPG and the GLS coincide in the pure hyperbolic case, or for piecewise linear elements as discussed in the same work. The SUPG and the GLS methods have been related to the process of addition and elimination of suitable bubble functions (Brezzi, 1992; Baiocchi and Brezzi, 1993). Then, Brezzi and Russo (1994) started the residual-free bubble (RFB) approach, which is further developed by Franca and Russo ((1996 .In the present work, the SUPG technique is used to solve the flow equations to treat the convective nature of the momentum equations while the standard Galerkin technique is used to solve the modified continuity equation since it is of an elliptic type. The wall deformation problem is modeled using the variational approach. The hybrid technique is used to model and simulate the pulsatile blood flow problem in a deformable artery.

2. THE MATHEMATICAL MODEL

For non-polar Newtonian, incompressible fluids, with no heat or mass addition; the continuity and momentum equations in non-dimensional form read:

$$\nabla \cdot \mathbf{V} = 0 , \tag{1}$$

$$d\mathbf{V} / dt = -\nabla P + 1 / R_e \nabla^2 \mathbf{V} , \tag{2}$$

Where $\mathbf{V}$ is the velocity vector, t is time, P is the pressure, R_e is the Reynold's number.

2.1 The Incompressibility Constraint

A well-known problem in the numerical treatment of incompressible formulation is how to treat the incompressibility constraint as the continuity equation becomes a constraint equation for the velocity field rather than being an evolution equation for the density field. The algorithm developed by Habashi and Baruzzi (1989) to approximately satisfy the incompressibility constraint is adopted in the present study. The continuity equation is modified to:

$$\nabla \cdot \mathbf{V} = \varepsilon \nabla^2 P , \tag{3}$$

where ε is the pressure stabilization controlling parameter. The main gain of this modification is that equal order shape functions could be safely used for all variables as well as the same integration scheme.

2.2 The elastic Boundary Model

The deformation of the boundary is accounted for by considering the boundary as a simply supported beam under transverse unsteady distributed load namely, the fluid pressure. Applying the principle of Minimum Potential Energy (MPE) (Arthur *et al.*, 2011) to the case of bending of a symmetric beam in a regime of small deflection, the functional of the total Potential Energy U in the dimensionless form is (Boraey *et al.*, 2015):

$$U(t)=\int_0^{L/D}\left[\frac{EI}{2\rho u_\infty^2 D^4}\left(\frac{\partial^2 w}{\partial x^2}\right)^2+q(x;t)w\right]dx\,, \tag{4}$$

where L is the artery length, D is the artery inlet diameter, E is is the modulus of elasticity, I is the moment of area, ρ is the blood density, u_∞ is the maximum of the inlet velocity, w is the artery wall deflection, q is the fluid pressure at the artery wall.

The non-dimensional parameters are: the inlet diameter D, the blood density ρ and u_∞ . The resulting nondimensional numbers are the Reynold's number given by $R_e=\frac{\rho u_\infty D}{\mu}$ and a new number which we called Index of Fluid-Structure Interaction (ISFI) given by:

$$ISFI=EI/\rho u_\infty^2 D^4\,, \tag{5}$$

Which is the ratio of boundary flexural rigidity to the fluid momentum flux. *ISFI* equals infinity for a rigid boundary.

3. Numerical Technique and Discretization

The finite element method is used to solve the fluid model as well as the structural model. The variational approach is used in modeling the structural problem while the Galerkin technique is used for the continuity equation. But due to the convective nature of the momentum equation, the SUPG technique is adopted to stabilize the solution.

3.1 Finite Element Model of the Fluid Flow

The weak form of the modified continuity equation using the standard Galerkin technique is:

$$\int_A\left[(\nabla\cdot\mathbf{V})N_i+\varepsilon(\nabla P\cdot\nabla N_i)\right]dA-\oint_{\partial A}\varepsilon N_i\,\partial P/\partial\mathbf{n}\,d\mathbf{s}=0\,, \tag{6}$$

Where N_i are the shape functions and **n** is the outward unit normal to the boundary. The weak form of the momentum equation using the SUPG formulation is:

$$\int_A\left[\mathbf{W}_i\frac{\partial\mathbf{V}}{\partial t}+\mathbf{W}_i(\mathbf{V}\cdot\nabla\mathbf{V})+1/R_e(\nabla\mathbf{V}\cdot\nabla\mathbf{N}_i)-\mathbf{N}_i\nabla P\right]dA-\oint_{\partial A}1/R_e\,\mathbf{N}_i\,\partial\mathbf{V}/\partial\mathbf{n}\,d\mathbf{s}=0 \tag{7}$$

In which $\mathbf{N}_i=N_i\mathbf{I}$, and $\mathbf{W}_i=W_i\mathbf{I}$ with **I** being the identity matrix. A discontinuous term is added to the Galerkin standard weighting function, for stabilization purposes, as follows (Brooks and Hughes, 1982):

$$W_i=N_i+p_i\,, \tag{8}$$

where p_i is the discontinuous streamline upwind contribution defined as:

$$p_i=\frac{k}{\|\mathbf{V}\|}(\mathbf{V}\cdot\nabla N_i)\,, \tag{9}$$

where k is an artificial diffusivity controlling parameter and **V** is calculated at the element center.

3.2 Finite Element Model of the Boundary Deformation

The variational approach is used to reach the element equations for the boundary deformation problem. The nodal unknowns in vector form are:

$$\mathbf{w}=[w_1\quad\theta_1\quad w_2\quad\theta_2]\,, \tag{10}$$

where $\theta=\partial w/\partial x$ is the slop of the deflection. Introducing the finite element approximation for the nodal unknowns:

$$\mathbf{w}=S_i\,\mathbf{w}_i\,, \tag{11}$$

where S_i are the cubic shape functions (Boraey *et al.*, 2015). Minimization of the functional given in equation Eq. (4) after introducing the finite element approximation, Eq. (4) yields the element matrix form:

$$[k]\{w\}=\{r\}\,, \tag{12}$$

where the matrices in Eq. (12) are:

$$[k]=\frac{IFSI}{l_e^3}\begin{bmatrix}12 & 6l_e & -12 & 6l_e\\ 6l_e & 4l_e^2 & -6l_e & 2l_e^2\\ -12 & -6l_e & 12 & -6l_e\\ 6l_e & 2l_e^2 & -6l_e & 4l_e^2\end{bmatrix}, \tag{13}$$

and

$$\{r\}=\frac{q(x;t)l_e}{2}\{-1\quad l_e/6\quad -1\quad l_e/6\}^T\,, \tag{14}$$

All the integrations are carried out numerically using 3-ponits Gauss-Legendre quadrature.

3.3 Time Marching Scheme

Let $[0, t_f]$ be the time zone over which the behavior of the artery is observed, and $0=t_0<t_1<\ldots<t_N=t_f$ be a partition of $[0, t_f]$, where $\Delta t = t_n - t_{n-1}$ is the amplitude of the time interval $[t_{n-1}, t_n]\subset [0, t_f]$, for $n = 1,\ldots N$, and N is the total number of these subintervals. Since we are interested in a time accurate solution and consequently a small time-step is used, a forward Euler first order scheme is used to overcome the nonlinearity due to the convective terms in the momentum equation as well as to decouple the system of equations resulting in less computer memory requirements. Brooks and

Hughes (1982) show that the mass matrix *M*, the matrix multiplied by the velocity time derivative, in Eq. (7) is affected by the time marching scheme and consequently its definition is determined according to which part of the system of equations is treated implicitly or explicitly. Hence for the case at hand, in which we treat everything explicitly, this matrix is replaced by its diagonal form as explained by Brooks and Hughes (1982).

4. RESULTS AND DISCUSSION

Pulsating blood flow problem is solved considering two cases namely a rigid artery and an elastic artery. The results of the current contribution compare well compared to the available published data. Before we present the results of the main problem in the current contribution, a mesh independent test is performed to make sure of the behavior of the developed in-house code with mesh refinement. The well-known benchmark problem lid-driven cavity is used for the code testing. Figure 1 shows the axial velocity compared to the experimental work of Pakdel *et al.* (2001). The figure shows that the finer the mesh the closer the resulting numerical solution to the experimental work.

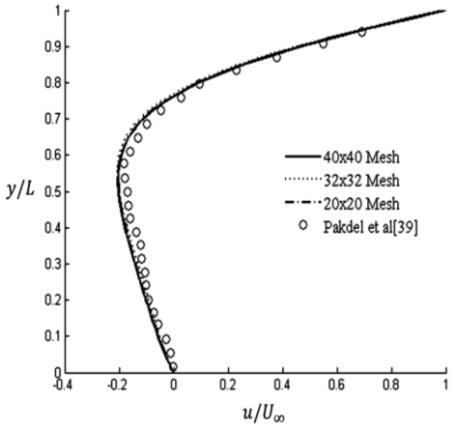

Fig. 1. Mesh-independent test using the *x*-component velocity at *x*=0.5 for *Re* ≈ 0.

4.1 Pulsating Blood Flow

The pulsating blood flow problem (PBF) in a rigid and elastic artery is considered. A pulsatile flow is one of the most important types of unsteady flows in which the inlet and/or outlet flow boundary conditions are modeled as a wave propagating in or out of the domain of interest. The most crucial application to this type of flows is the study of the dynamics of blood flow in elastic arteries. Flow in an artery is best described by cylindrical coordinates. However, as a first approximation, in the current study the flow in elastic tube is approximated by two-dimensional planar flow. The constitutive equation describing the response of blood to external stimuli depends on many factors, the most important of which are: i) the relative size of the domain, in which the blood is flowing, to the size of blood constituents e.g. platelets, white blood cells, …etc. ii) the physical phenomena we need to include in the simulation e.g. shear-thinning behavior, clotting, fluid fading memoryetc. In general, blood is considered as a thixotropic viscoelastic incompressible fluid (Zamir, 2005). The size of the arteries is varying considerably and consequently affects the choice of the blood constitutive model. In the case of large arteries e.g. carotid, the blood is exposed to high shear rates and so could be considered as a Newtonian fluid (Zamir, 2005; Kim, 2009; Nichols *et al.*, 2011). It is believed that blood could be considered as a Newtonian fluid at shear rates above 100 *s*-1 (Marrero *et al.*, 2014). On the other hand, in small arteries and tissues other models should be considered. The scope of the current work is the study of the hemodynamics in the carotid artery in which the Newtonian assumption could be safely adopted.

4.2 Problem Description

The physical domain of interest which is a carotid artery is modeled with the following data: 0.3 *cm* radius, 12.6 *cm* length and 0.03 thickness. The artery wall properties are: Young's Modulus of 0.407 *MPa* and density of 1000 kg/m^3 (Figueroa *et al.*, 2006). While the Newtonian properties of the blood are: density of 1060 kg/m^3 and dynamic viscosity of 4E-3 *Pa.s* (Figueroa *et al.*, 2006). The computational domain and the grid used in the simulation are presented in Fig. 2 in which 25 x 75 bilinear quadrilateral elements are used for the geometry as well as for all the flow variables with a total number of nodes of 1976. The inlet pulsating flow rate is calculated by an analytical formula provided by Nichols *et al.* (2011) in which the pressure gradient is assumed as a harmonic function resulting in the following analytical form for the blood volumetric flow rate:

$$Q = \sum_{i=1}^{n} \frac{D^2 A_i A_i^o}{4\mu\alpha_i^2} \sin\left(\omega_i t - \phi_i + \varepsilon_i\right), \tag{15}$$

where Q is the volume flow rate, n is the number of harmonics, ω is the frequency, (ϕ_i, ε_i, A) are constants depending on the nondimensional number α known as Womersley number. This number is the main parameter affecting pulsatile flows and is defined as (Nichols *et al.*, 2011):

$$\alpha_i = 0.5D\sqrt{\omega_i \rho/\mu}\ , \tag{16}$$

The resulting volumetric flow rate has a periodic time T=1.37 sec and maximum volumetric flow rate of 12.18 cc/sec. The R_e= 685 based on the maximum inlet velocity as the characteristic velocity.

Fig. 2. Finite element mesh of the Carotid artery model.

4.3 Boundary and Initial Conditions

The no-slip condition is imposed on the upper and lower walls. The pulsating flow rate wave used as the inlet boundary condition and for the outlet the

pressure is set to 85 mmHg. The initial conditions are zero for the velocity boundary nodes. In the following two subsections, two cases are considered; the first is the blood flow in rigid artery while in the second case the artery elasticity is considered.

4.4 Pulsating Blood Flow in a Rigid Artery

The numerical values for the artificial viscosity are ε=0.0005 and a time step of 0.0004. The following results are for a total time of two periods which corresponds to 6900 time-steps. The evolution of pressure and volumetric flow rate is traced in two cross-sections namely; S1 and S2 where S1 is just one spatial step away from the inlet boundary at the centerline and S2 is located one spatial step ahead of the exit section. Figure 3 shows the pressure as well as the volumetric flow rate distribution. The time delay between the leading pressure wave and the volumetric flow rate wave is approximately $\Delta t_{lead} \approx 0.15$ sec. The flow rate wave is presented in Fig. 4 at both locations S1 and S2 as well as the pressure in Fig. 5. The results show that the mean flow value at S2 is less than the mean flow at S1. The velocity profiles at different axial locations (A, B, C, D, E and F) for different time points over the flow wave period is presented in Fig. 6. These results are consistent with the conclusion reached by Kim (2009) in that the backflow occurs around point D shown in Fig. 6.

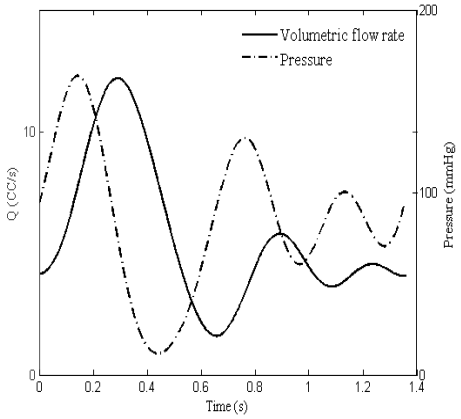

Fig. 3. Pulsating inlet flow rate and pressure.

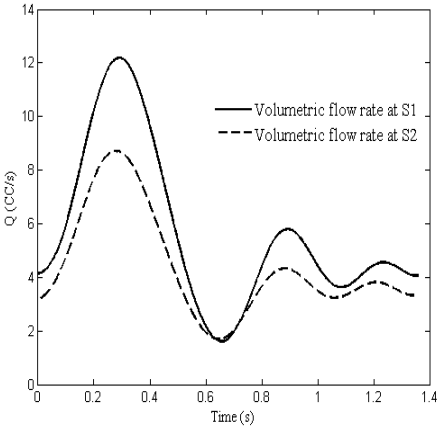

Fig. 4. Volumetric flow rate at both S1 and S2.

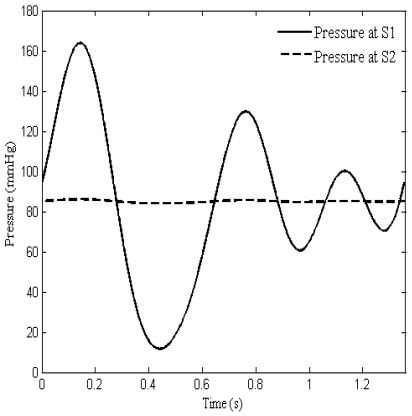

Fig. 5. Pressure distribution at both locations S1. And S2.

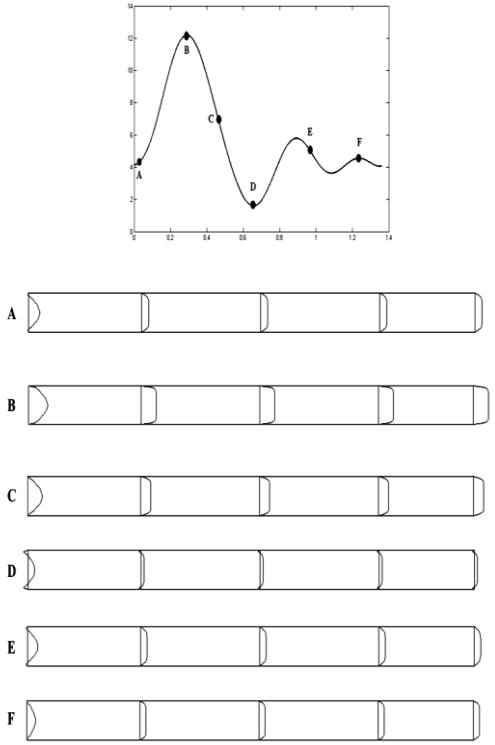

Fig. 6. Velocity profiles at different axial locations for different time stations.

4.5 Pulsating Blood Flow in an Elastic Artery

In this section the deformability of the boundary is considered. The elastic boundary model is used considering the fluid pressure as the external load. Due to the problem symmetry, the deflection of the upper boundary is calculated only. Using the same numerical values for the time step as well as for the pressure stabilization parameter. the presented solution is obtained after 6900 time-steps. In Fig. 7, the deflection variation and the pressure wave are plotted at five sections along the artery (B1, B2, B3, B4 and B5). B1 and B5 are at the same axial location of S1 and S2 respectively but on the upper wall. The other three axial locations B2, B3 and B4 are at *x*=3.36, *x*=6.3, *x*=8.36 *cm* respectively. For

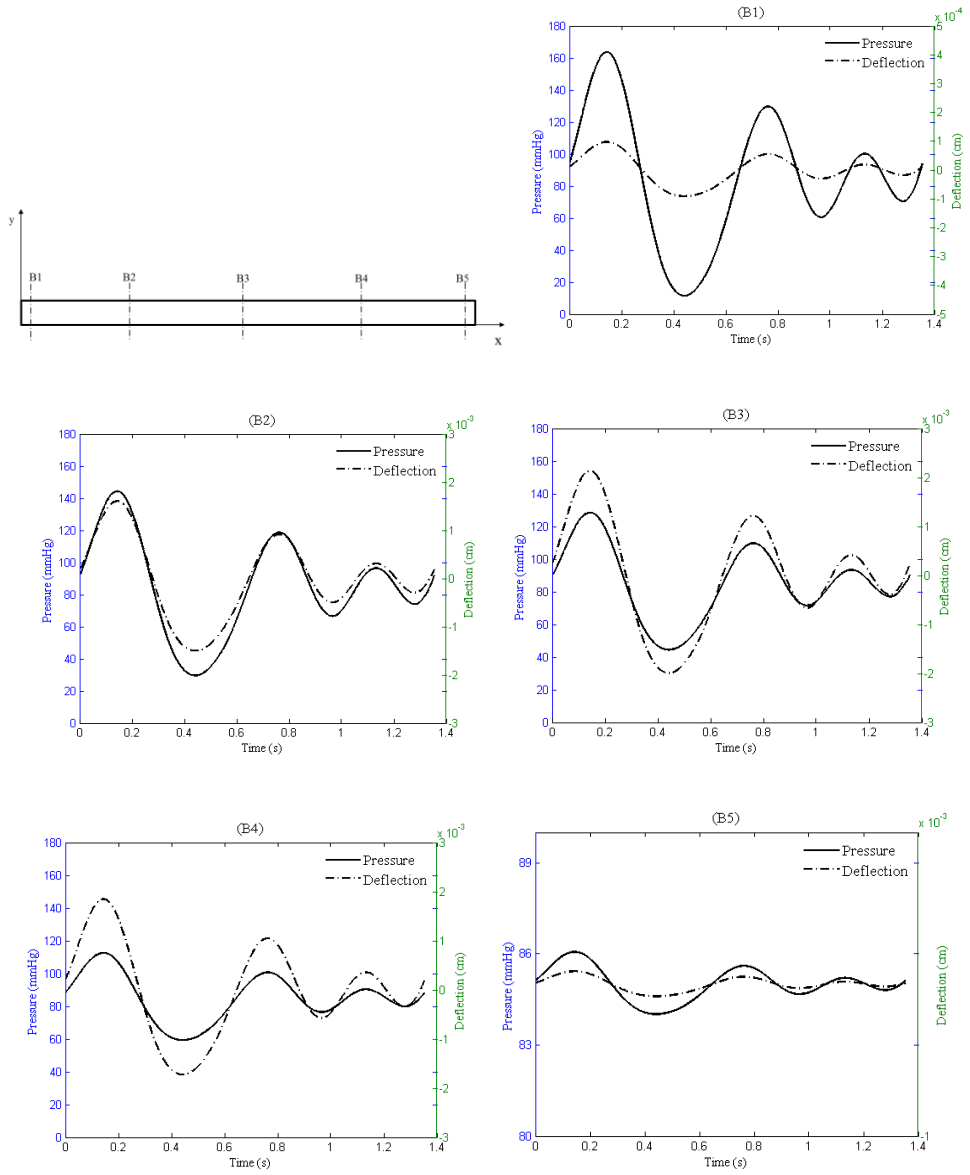

Fig. 7. Pressure and deflection of the artery wall at different spatial locations B1 through B5.

further details the deflection of the whole boundary is shown in Fig. 8 at different time points (B and C) over the inlet pressure wave period and the deflection flooded by the pressure field. These results are consistent with the conclusion reached by Figueroa *et al.* (2006) in that the pressure and deflection waves are in-phase. Also, the leading time of the pressure wave is $\Delta t_{lead} \approx 0.15$ sec while it for Figueroa *et al.* (2006) $\Delta t_{lead} \approx 0.13$ sec. The maximum deflection is found to be $w_{\max} \approx 0.003\,cm$ compared to $w_{\max} \approx 0.005\,cm$ for Figueroa *et al.* (2006). To show the importance of taking the wall elasticity into account; the pressure fluctuation at B1 and the wall shear stress at B3 is plotted in Fig. 9 and Fig. 10 respectively for the case of rigid wall and deformable wall at two *IFSI* numbers. The results show that decreasing the *IFSI* number is highly affecting the pressure distribution as well as the wall shear stress.

5. SUMMARY AND CONCLUSIONS

A new model for simulating pulsatile incompressible viscous flow in elastic tubes is successfully developed and implemented. The incompressibility constraint problem is treated by the artificial viscosity technique developed by Habashi and Baruzzi (1989). The Newtonian assumption is shown to be accurate enough to represent the blood behavior in large arteries. The streamline/upwind Petrove-Galerkin finite element technique is shown to be effective and robust in treating the convective nature of the equations. The two-way coupling between the flow field and the boundary elasticity is accounted for by considering the wall as a simply supported beam under unsteady distributed load. The main results of this contribution are: (1) The artery wall pressure is overestimated when assuming a rigid artery while (2) The wall shear stress is underestimated, (3) The

importance of the wall deformability is found to be dependent on the *IFSI* non-dimensional number which is the ratio of boundary flexural rigidity to the fluid momentum flux. As a future work, extending the model to be three-dimensional would greatly enhance the results. As well as different types of boundary condition on the artery exit are to be considered e.g. impedance and resistance boundary condition.

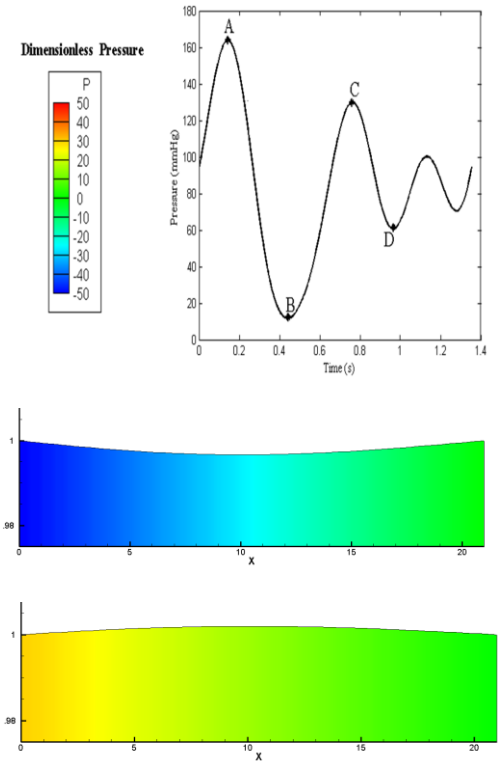

Fig. 8. Shape of the artery wall at different time stations (B and C) flooded by the pressure field

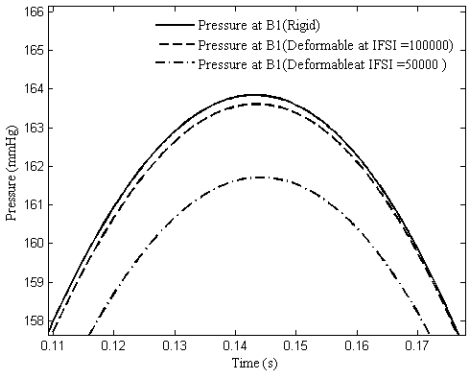

Fig. 9. Pressure wave at B1 for rigid and deformable wall.

ACKNOWLEDGEMENTS

The authors would like to thank Cairo University and Nile University for their support.

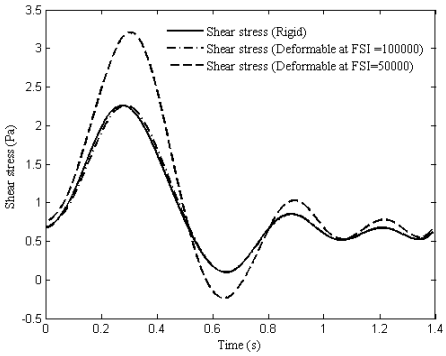

Fig. 10. Wall shear stress at B3 for rigid and deformable wall at different *IFSI* numbers.

REFERENCES

Ait-Ali-Yahia D, W. G. Habashi, A. Tam, M.-G. Vallet, and M Fortan (1996). A Directionally Adaptive Methodology Using an edge-based error estimate on quadrilateral grids. *International. Journal for Numerical Methods in Fluids*, 23, 673-690.

Arthur, R. B., P. C. Ken, D. L. James (2011). *Elasticity in Engineering Mechanics*. 3rd ed. John Wiley and Sons, New York, USA.

Baiocchi, C. and F. Brezzi (1993). Virtual bubbles and Galerkin-least-squares type methods. *Computer Methods in Applied Mechanics and Engineering* 105, 125–141.

Bo W., X. Liu, J. Glimm, and X. Li (2011). A robust front tracking method: verification and application to simulation of the primary breakup of a liquid jet. *SIAM Journal on Scientific Computing*, 33(4), 1505-1524.

Boraey M., A. Guaily and M. Epstein (2015). A Hybrid Model for Biofilm Growth on A Deformable Substratum. *The Canadian Journal of Chemical Engineering*, 93, 789–797.

Brezzi F. and A. Russo (1994) Choosing Bubbles for Advective-Diffusion Problems. *Mathematical Models and Methods in Applied Sciences*, 4(4), 571–587.

Brezzi F., Mallet M. and G. Rog (1992). A relationship between stabilized finite element methods and the Galerkin method with bubble functions. *Computer Methods in Applied Mechanics and Engineering*, 96, 117–129.

Brooks N. and T.J.R. Hughes (1982). Streamline Upwind/Petrov-Galerkin Formulations for Convective Dominated Flows with Particular Emphasis on the Incompressible Navier-Stokes Equations. *Computer Methods in Applied Mechanics and Engineering*, 32, 199–259.

Deparis S., Fernandez M. A. and L. Formagia (2003). Acceleration of a fixed-point algorithm for fluid-structure-interaction using transpiration conditions. *ESAIM:M2AN*, 37,

601–616.

Donea J., S. Giuliani and J. P. Halleux (1982). An arbitrary Lagrangian-Eulerian finite element method for transeint dynamic fluid-structure interactions. *Computer Methods In Applied Mechanics and Engineering*, 33, 689–723.

Enriquez-Remigio S. A., and A. M. Roma (2005). Incompressible flows in elastic domains: an immersed boundary method approach. *Applied Mathematical Modelling*, 29, 35–54.

Fernández M. Á., and P. L. Tallec (2003). Linear stability analysis in fluid–structure interaction with transpiration. part II: numerical analysis and applications. *Computer Methods in Applied Mechanics and Engineering*, 192, 4837–4873.

Figueroa C. A., Vignon-Clementel I. E., K. E. Jansen, T. J. R. Hughes and C. A. Taylor (2006). a coupled momentum method for modeling blood flow in three-dimensional deformable arteries. *Computer Methods in Applied Mechanics and Engineering*, 195, 5685–5706.

Franca L. P. and A. Russo (1996). Deriving upwinding, mass lumping and selective reduced integration by residual-free bubbles. *Applied Mathematics Letters*, 9 (5), 83–88.

Guaily A, and A. Meghed (2010). An adaptive finite element method for planar and axisymmetric compressible flows. *Finite Elements in Analysis and Design*, 46(8), 613-624.

Guaily A, and M. Epstein (2010). A unified hyperbolic model for viscoelastic liquids. *Mechanics Research Communications*, 37(2), 158-163

Habashi W. G. and G. S. Baruzzi (1989). A Newton-Galerkin algorithm for computational fluid dynamics. *In Proceedings of International Symposium on Computational Fluid Dynamics*, 3rd volume, 347–352.

Hart J. De, F. P. T. Baaijens, G. W. M. Peters, P. J. G. Schreurs (2003). A Computational fluid-structure interaction analysis of a fiber-reinforced stentless aortic valve. *Journal of Biomechanics*, 36, 699–712.

Hughes J. R. and K. Zimmermann (1981). Lagrangian-Eulerian finite element formulation for incompressible viscous flows," *Computer Methods In Applied Mechanics and Engineering*, 29, 329–349.

Hughes T.J.R., and L. P. Franca (1989). A new finite element formulation for computational fluid dynamics: VIII. the Galerkin/least-squares method for advective-diffusive equations. *Computer Methods in Applied Mechanics and Engineering*, 73, 173–189.

Kelidis P., and E. Konstantinidis (2018). Pulsatile flow through a constricted tube: effect of stenosis morphology on hemodynamic parameters. *Computer Methods Biomechanics Biomedical Engineering* 21(7), 479-487.

Kelly J. M., C. Picioreanu, and R. Nerenberg (2013). Multidimensional modeling of biofilm development and fluid dynamics in a hydrogen-based, membrane biofilm reactor (MBfR). *Water Research*, 47(13), 4739-4751.

Kim H. J. (2009). *Three-dimensional finite element modeling of blood flow in the coronary arteries*," Ph. D. thesis, Stanford University, USA.

Lynn P. P. and S. k. Arya (1973). Use of the least squares criterion in the finite element formulation. 6, 75–88.

Ma M., J. Lu, and G. Tryggvason (2015). Using Statistical Learning to Close Two-Fluid Multiphase Flow Equations for a Simple Bubbly System. *Physics of Fluids*, 27, 092101.

Ma M., J. Lu, and G. Tryggvason (2016). Using statistical learning to close two-fluid multiphase flow equations for bubbly flows in vertical channels. *International Journal of Multiphase Flow*. 85, 336-347.

Mao W., A. Caballero, R. McKay, C. Primiano and W. Sun (2017). Fully-coupled fluid-structure interaction simulation of the aortic and mitral valves in a realistic 3D left ventricle model. *PLoS ONE* 12(9): e0184729.

Marrero V. L., J.A. Tichy, O. Sahni, and K. E. Jansen (2014). Numerical study of purely viscous non-Newtonian flow in abdominal aortic aneurysm. *Journal of Biomechanical Engineering*, 136, 1-10.

Nichols W. W., M. F. O'Rourke, C. Vlachopoulos (2011). McDonald's *Blood Flow in Arteries Theoretical, Experimental and Clinical Principles*, 6th ed. London, United Kingdom: Hodder Arnold.

Pakdel P., S. H. Spiegelberg, and G. H. Mckinley (2001). Cavity Flows of Elastic Liquids: Two-Dimensional Flows. *Journal of Physics of Fluids*, 9, 3123–3140.

Peskin S. (1977). Numerical analysis of blood flow in the heart. *Journal of computational physics* 25, 220-252.

Popinet S., and S. Zaleski (1999). A front tracking algorithm for accurate representation of surface tension. *International Journal for Numerical Methods in Fluids*. 30(6), 775-93.

Raju G., V. Mallela, and A. Quiroga (2017, November). Applications of Fluid Structure Interaction Analysis Techniques for Flow Regulation. *Proceedings of the ASME International Mechanical Engineering Congress and Exposition. Tampa, Florida, USA.*

Sugiyama K., S. Ii, K. Shimizu, S. Noda, and S. Takagi (2017). A full Eulerian method for

fluid-structure interaction problems. *Procedia IUTAM*, 20, 159-166.

Taghaddosi F., W. G. Habashi, G. Guevremont and D. Ait-Ali-Yahia (1999). An adaptive least-squares method for the compressible euler equations. 1139, 1121–1139.

Tryggvason G., M. Ma, and J. Lu (2016). DNS-Assisted Modeling of Bubbly Flows in Vertical Channels. *Nuclear Science and Engineering*, 184, 312-320.

Zamir M. (2005). *The Physics of Coronary Blood Flow*. Springer, Ontario, Canada.